Received: 6 May 2019 | Revised: 10 September 2019 | Accepted: 11 September 2019

DOI: 10.1111/jace.16805

Journal of the American Ceramic Society

ORIGINAL ARTICLE

Insight into cations substitution on structural and electrochemical properties of nanostructured Li_2FeSiO_4/C cathodes

Pazhaniswamy Sivaraj[1,2] | **Karuthedath Parameswaran Abhilash**[3] | **Balakrishnan Nalini**[4] | **Paneerselvam Christopher Selvin**[1] | **Sunkulp Goel**[3] | **Sudheer Kumar Yadav**[3]

[1]Solid State Ionics and Luminescence Laboratory, Department of Physics, Bharathiar University, Coimbatore, India

[2]Materials Research Centre, Department of Physics, N. G. M. College, Coimbatore, India

[3]Herbert Gleiter Institute of Nanoscience, Nanjing University of Science and Technology, Nanjing, China

[4]Department of Physics, Avinashilingam Institute for Home Science and Higher Education for Women, Coimbatore, India

Correspondence
B. Nalini, Department of Physics, Avinashilingam Institute for Home Science and Higher Education for Women, Coimbatore 641043, India.
Email: jyothsnalalin99@gmail.com

P. Christopher Selvin, Solid State Ionics and Luminescence Laboratory, Department of Physics, Bharathiar University, Coimbatore 641046, India.
Email: csphysics@buc.edu.in

Funding information
Council of Scientific Industrial Research (CSIR), Govt. of India, Grant/Award Number: 09/0472(0181)2018-EMR-I

Abstract

Structural instability is the major obstacle in the Li_2FeSiO_4/C cathode during charge and discharge process, which can be improved by the substitution of cations in the host cage. In this study, the transition metal ions with different valence (Ag^{1+}, Zn^{2+}, Cr^{3+}, and Ti^{4+}) have been substituted in Li_2FeSiO_4/C via modified sol-gel method and the impact on the structural, electrical, and electrochemical performances has been systematically explored. The Rietveld-refined XRD pattern and HR-TEM (SAED) result reveal that all the prepared samples maintain orthorhombic structure (S.G- $Pmn2_1$). The FE-SEM and TEM micrographs of bare and doped Li_2FeSiO_4/C display nanoparticle formation with 20-40 nm size. Among different cation-substituted silicates, $Li_2Fe_{0.9}Ti_{0.1}SiO_4$/C sample exhibits an excellent total conductivity of 1.20×10^{-4} S cm^{-1} which is one order of magnitude higher than the bare Li_2FeSiO_4/C sample. The galvanostatic charge-discharge curves and cyclic voltammetric analysis reveal that the $Li_2Fe_{0.9}Ti_{0.1}SiO_4$/C material provides an excellent initial specific capacity of 242 mAh g^{-1} and maintains a capacity of 226 mAh g^{-1} after 50 cycles with capacity retention of 93.38%. The Ti doping is a promising strategy to overcome the capacity fading issues, by preventing the structural collapse during Li-ion intercalation/de-intercalation processes in the Li_2FeSiO_4/C electrode through the strong hybridization between the 3*d* and 4*s* orbitals in titanium and 2*p* orbital in oxygen.

KEYWORDS
doping, electrochemical performance, Li_2FeSiO_4/C, lithium ion batteries, nano cathode

1 | INTRODUCTION

Metal orthosilicates, Li_2MSiO_4 (M = Fe, Mn, Co, etc) have emerged as the high capacity cathode materials owing to their tremendous advantages such as good theoretical capacity (332 mAh g^{-1}), two Li-ion extractions per formula unit, high thermal stability, and the environmental benignity.[1,2] Among these orthosilicates, Li_2FeSiO_4 (LFSO) exhibits good electrochemical activity and best cycling stability,[3,4] which is considered as one of the most promising alternative cathode materials for next-generation advanced lithium-ion batteries. This material possesses an excellent voltage window, best energy storage capability, safe operation, and environmental friendliness due to the presence of Fe and Si ion combination in its structural unit. The cost-effective LFSO cathode material with the stable structure

created significant attention when compared with the existing conventional cathodes such as $LiMO_2$ (M = Ni, Co, and Mn), $LiMn_2O_4$, and olivine-type $LiFePO_4$.[5] The lower electronegativity of Si (2.03) in Li_2FeSiO_4 when compared with P (2.39) in the $LiFePO_4$ cathode,[3] can effectively reduce de-intercalation voltage during the formation of Fe^{2+} to Fe^{3+} redox pair.[3] Despite many advantages, the LFSO suffers from low electronic/ionic conductivity, poor diffusion rate (~10^{-17} cm^{-1}), structural distortion, and capacity fading which limits high rate electrochemical performances when used as the cathode material for LIBs.[6,7]

Numerous strategies have been employed to improve the electrical and electrochemical performance of LFSO nano cathode, which include the reduction of particle size into the nanoscale, making porous morphology, carbon coating (through citric acid, sucrose, PVP, Pluronic 123, etc), and supervalent cation doping.[8] Among these approaches, the aliovalent/isovalent metal ion doping is being considered as an effective strategy to enhance the intrinsic electronic/ionic conductivity, structural stability, and electrochemical performances of LFSO matrix. Several researchers have investigated the impact of the substitution of Mn^{2+}, Mg^{2+}, Zn^{2+}, Cu^{2+}, Cr^{3+}, Ni^{2+}, V^{3+} metal ions and its structural and electrochemical impact on LFSO.[8–11] Deng et al had investigated the effects of Zn^{2+}, Cu^{2+}, and Ni^{2+} dopant on the physical and electrochemical properties of LFSO and reported that the Zn^{2+}-doped sample exhibits better electrochemical performances.[12] Zhang et al studied the effects of Cr^{3+} doping on the electrochemical characteristics of LFSO and the doped sample with 3% Cr^{3+} exhibited better discharge capacity.[13] Recently, Hailong Qiu et.al reported that 2% Ti-doped LFSO possess better electrochemical performance with a discharge capacity of 102.8 and 91.1 mAh g^{-1} at current rates of 5 and 10 C, respectively.[14]

Even though some researchers have reported the cations doping in Li_2FeSiO_4, there is no report on the investigation of the influence of oxidation state of cations on Li_2FeSiO_4 cathodes. In addition, the previous studies fail to state the reason behind the improvements in the electrochemical performances of the Li_2FeSiO_4 by doping of aliovalent cation, which is still under investigation. The oxidation state of dopant element and different synthesis parameters such as raw materials, calcination temperature, and preparation procedure play a major role to examine the electrochemical performance of the cathode material. Hence, it is necessary to investigate the impact of the oxidation state of dopant elements on the Li_2FeSiO_4 by a single preparation method. The present study not only identifies the significance of the best dopant ions to strengthen the structural and electrochemical properties of Li_2FeSiO_4 cathode, but also the reason behind the improvement of electrochemical properties has been investigated. For the first time, it has been attempted to incorporate four different cations with the increase in the order of valence (Ag^{1+}, Zn^{2+}, Cr^{3+}, and Ti^{4+}) at the Fe site of the Li_2FeSiO_4 and systematically explored the results. The effective incorporation of these elements in the Li_2FeSiO_4 host matrix without disturbing its fruitful orthorhombic structure ($Pmn2_1$) deserves the scientific attention.

2 | EXPERIMENTAL PROCEDURE

2.1 | Material preparation

The LFSO/C nanoparticles have been synthesized using a modified sol-gel method. The $LiCH_3COOH{\cdot}2H_2O$ (Sigma Aldrich, reagent grade 99.55%), $Fe(NO_3)_3.9H_2O$ (Sigma Aldrich, 99.9%), Tetraethyl orthosilicate-$Si(OC_2H_5)_4$ (TEOS) (Sigma Aldrich, purity of 99.995%), and P123 polymer were used as raw materials. The lithium acetate (4.08 g: 0.04 mol) and iron nitrate nonahydrate (8.08 g: 0.02 mol) were dissolved in 50 mL of distilled water under vigorous stirring. The TEOS (4.17 g: 0.02 mol) was dissolved in 20 mL ethanol separately and stirred well. The dissolved TEOS solution was mixed with the above solution and stirred well to get a homogeneous mixture. In this solution, 1 g of P123 polymer was added under continuous stirring. The homogeneously mixed solution was heated at 80°C under constant magnetic stirring until getting a brown gel-like low viscous solution. The gel solution was kept overnight at 85°C in a furnace for the solvent evaporation. The resultant precursor was further calcined at 700°C in a tubular furnace under N_2 atmosphere over 10 hours to obtain the undoped LFSO/C nanopowder. Appropriate ratios of silver nitrate (purity > 99.93%), zinc nitrate (purity > 99.95%), chromium nitrate (purity > 99.93%), and tetrabutyl titanate (purity > 99.98%) were used as raw materials during the preparation step to incorporate the cations into host lattice using the same experimental procedures. The cations (Ag^{1+}, Zn^{2+}, Cr^{3+}, and Ti^{4+}) were doped at the Fe site of LFSO/C. The doped samples are designated as $Li_2Fe_{0.9}Ag_{0.1}SiO_4$/C, $Li_2Fe_{0.9}Zn_{0.1}SiO_4$/C, $Li_2Fe_{0.9}Cr_{0.1}SiO_4$/C, and $Li_2Fe_{0.9}Ti_{0.1}SiO_4$/C, respectively. A detailed report on the characterization techniques and electrochemical measurements (electrode fabrication and assembly of the aqueous electrochemical cell) of the samples has been provided as supplementary information (see Section S1).

3 | RESULTS AND DISCUSSION

3.1 | Structural and morphological characterizations

The XRD pattern of bare and cations (Ag^{1+}, Zn^{2+}, Cr^{3+}, and Ti^{4+})-doped LFSO/C nano cathode is shown in Figure 1A. The XRD peaks of bare LFSO/C can be assigned to

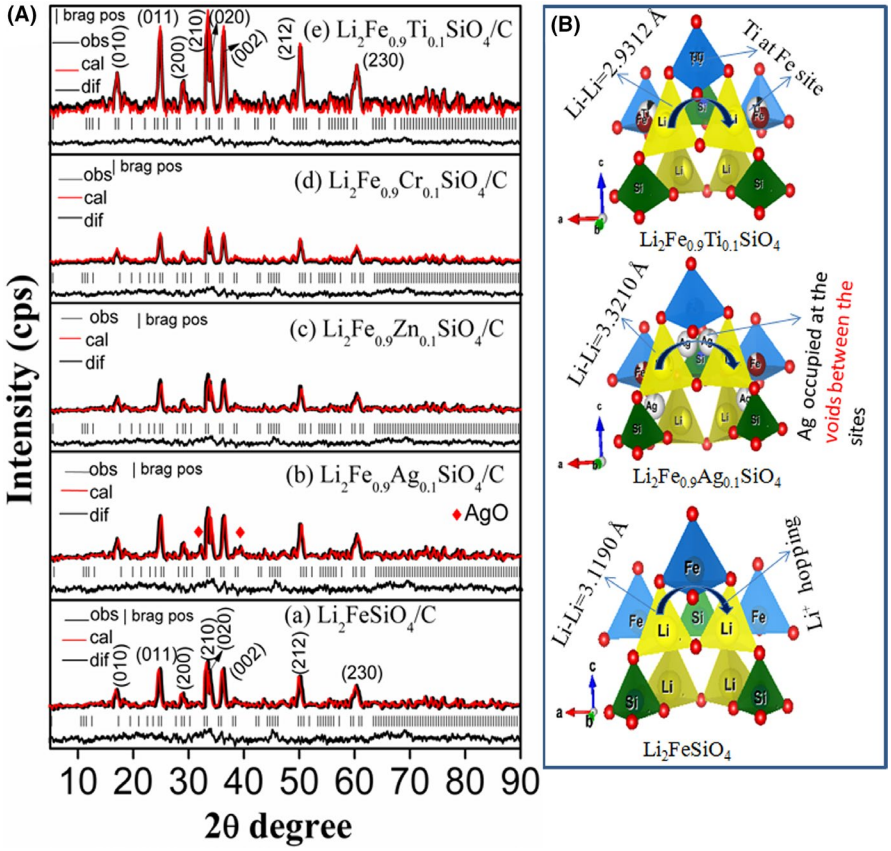

FIGURE 1 (A) Reitveld-refined XRD pattern of bare and metal ions (Ag^{1+}, Zn^{2+}, Cr^{3+}, and Ti^{4+}) doped Li_2FeSiO_4/C nano cathodes (not corrected for background) by GSAS software and (B) the refined crystal structure with Li–Li inter atomic distances in Ag^{1+}- and Ti^{4+}-doped LFSO/C samples

an orthorhombic structure (a = 6.27Å, b = 5.33Å, and c = 4.96 Å, $\alpha = \gamma = \beta = 90°$) with the $Pmn2_1$ space group which are consistent with the previous reports.[15,16] It is noticed that the LFSO/C does not exhibit any kind of impurities such as Fe_3O_4, Fe_2O_3, and $LiSiO_3$, which indicates the formation of a pure phase. The $Li_2Fe_{0.9}Ag_{0.1}SiO_4$/C cathode material possesses the same orthorhombic structure with the $Pmn2_1$ space group. However, it is found that two small diffraction peaks at 2θ = 32.17°, 39.34° are attributed to the AgO (ICDD:89-3081) impurity phase formed on the surface of LFSO/C host.

The Zn^{2+}, Cr^{3+}, and Ti^{4+} incorporated LFSO/C nanomaterials exhibit similar XRD pattern like the bare sample, which suggests that the Zn^{2+}, Cr^{3+}, and Ti^{4+} have occupied the cationic site of LFSO/C nanostructure without disturbing the parent crystal structure. The Zn^{2+}, Cr^{3+}, and Ti^{4+}-doped LFSO/C possess the orthorhombic structure ($Pmn2_1$) which directs that the di, tri, and tetravalent ions doping at Fe^{2+} site does not cause any impurity phase due to the low ionic radii of the Zn^{2+}, Cr^{3+}, and Ti^{4+}(0.64, 0.66, and 0.68Å) ions.[2,3] However, the intensity of the XRD pattern for LFSO/C decreases with the incorporation of Zn^{2+} and Cr^{3+} which may influence the crystallinity of the sample. In the $Li_2Fe_{0.9}Ti_{0.1}SiO_4$/C, the peak intensity is higher than that of other samples which indicates the better crystallinity of the sample. The high intensity in the XRD pattern of the $Li_2Fe_{0.9}Ti_{0.1}SiO_4$/C evidences the synergic interaction between the Ti^{4+} ions and the host matrix. There is no peak shift in the XRD pattern of bare and cation-doped LFSO/C cathodes which implicate the perfect incorporation of cations into the orthorhombic cage without amending the structural change.

The absence of the peak located at 2θ = 31.6°, corresponding to the (112) plan of the monoclinic phase[17] and the low-intensity ratio of the peaks at 2θ = 33.22/33.70° corresponding to (210)/(020) planes in the XRD pattern demonstrated that the prepared samples assume orthorhombic structure with the $Pmn2_1$ space group. It is very difficult to differentiate the orthorhombic phase with the $Pmn2_1$ space group from the monoclinic phase with $P2_1/n$ (coexisting with minor differences). Hence, the structures have been ascertained by Rietveld refinements using GSAS software and the refined lattice parameters are listed in Table S1. The Rietveld-refined XRD patterns implicate that the Zn^{2+}, Cr^{3+}, and Ti^{4+}-doped LFSO/C possess an orthorhombic structure similar to the $Pmn2_1$ space group without any impurity phase. The average crystallite size of the bare and Ag^{1+}, Zn^{2+}, Cr^{3+}, and Ti^{4+} ions-doped LFSO/C nano cathode are 20, 23, 15, 17, and 18 nm, respectively which follows the increasing order of the ionic radii (Zn (0.64 Å) < Cr (0.66 Å) < Ti (0.68 Å) < Ag (1.12 Å)) of different dopants.[11,13] The ionic radii play an important role in increasing/decreasing the crystallite size of

the LFSO/C sample.[18] Figure 1B shows the refined crystal structures, in which Ti incorporation effectively decreases the Li–Li hoping distance between the adjacent LiO_4 tetrahedron that favors facile Li-ion movement in the sample. Many of the previous studies report that the monoclinic structure of LFSO/C has been changed to a stable orthorhombic phase with better electrochemical properties after a few charge-discharge cycles.[17,19] This work reports a direct preparation of the stable orthorhombic structure ($Pmn2_1$) for bare and doped LFSO/C samples to obtain the best electrochemical performance with better cycling. The Ti^{4+} ion-doped LFSO/C sample shows better crystallinity in comparison with all other samples, which reflects in the electrical performance of the sample.

The XPS analysis has been performed to explore the oxidation state of the elements and the elemental composition of the samples (Figure 2). The binding energy scale for each specimen obtained in the XPS measurement has been calibrated using the binding energy of C 1*s* at 284.5 eV. The survey spectra of LFSO/C display the presence of Li, Fe, Si, O, C, and the doped samples confirm the presence of elements Ag, Zn, Cr and Ti in LFSO/C host matrix (Figure 2A-D and Figure S1A). As shown in Figure 2E, a peak at 368.3 eV, has been assigned to the Ag3$d_{3/2}$, which is consistent with the binding energy of Ag^{1+} in LFSO/C.[20] In the Zn^{2+} incorporated sample, a single peak has been observed with binding energy 1021.8 eV, originated due to Zn2$p_{3/2}$ state (Figure 2F).[21] In Figure 2G, a peak located with binding energy around 576.8 eV due to Cr 2*p* state is attributed to the oxidation state of Cr^{3+} in the host matrix.[13] A well-resolved peak centered at binding energy 458.1 eV in the $Li_2Fe_{0.1}Ti_{0.1}SiO_4$/C sample originates due to Ti2*p* and is attributed to the Ti^{4+} in an octahedral environment.[22] The existence of different valance state of Ag^{1+}, Zn^{2+}, Cr^{3+}, and Ti^{4+} ions in LFSO/C has been confirmed from the presence of Ag3*d*, Zn2*p*1/2, Cr2*p*, and Ti2*p* related peaks that occur in their respective XPS spectra. In addition, the binding energies of the Fe2*p*, Li1s, O1*s*, Si2*p* for Ag^{1+}, Zn^{2+}, Cr^{3+}, and Ti^{4+}-doped samples (Figure S1B-F) are very close to that of LFSO/C, which demonstrates that the metal ions doping does not change the oxidation state of Fe^{2+}, Li^{1+}, Si^{4+}, and O^{2-}. Moreover the C 1*s* XPS spectra originated a peak at 290 eV attributed to CO_3^{2-} which is evidence of the presence of Li_2CO_3, however, its intensity was found to be very small which indicated that the presence is only in trace amount.[23,24] The atomic % of the dopant elements (Ag^{1+}, Zn^{2+}, Cr^{3+}, and Ti^{4+}), that is present in the

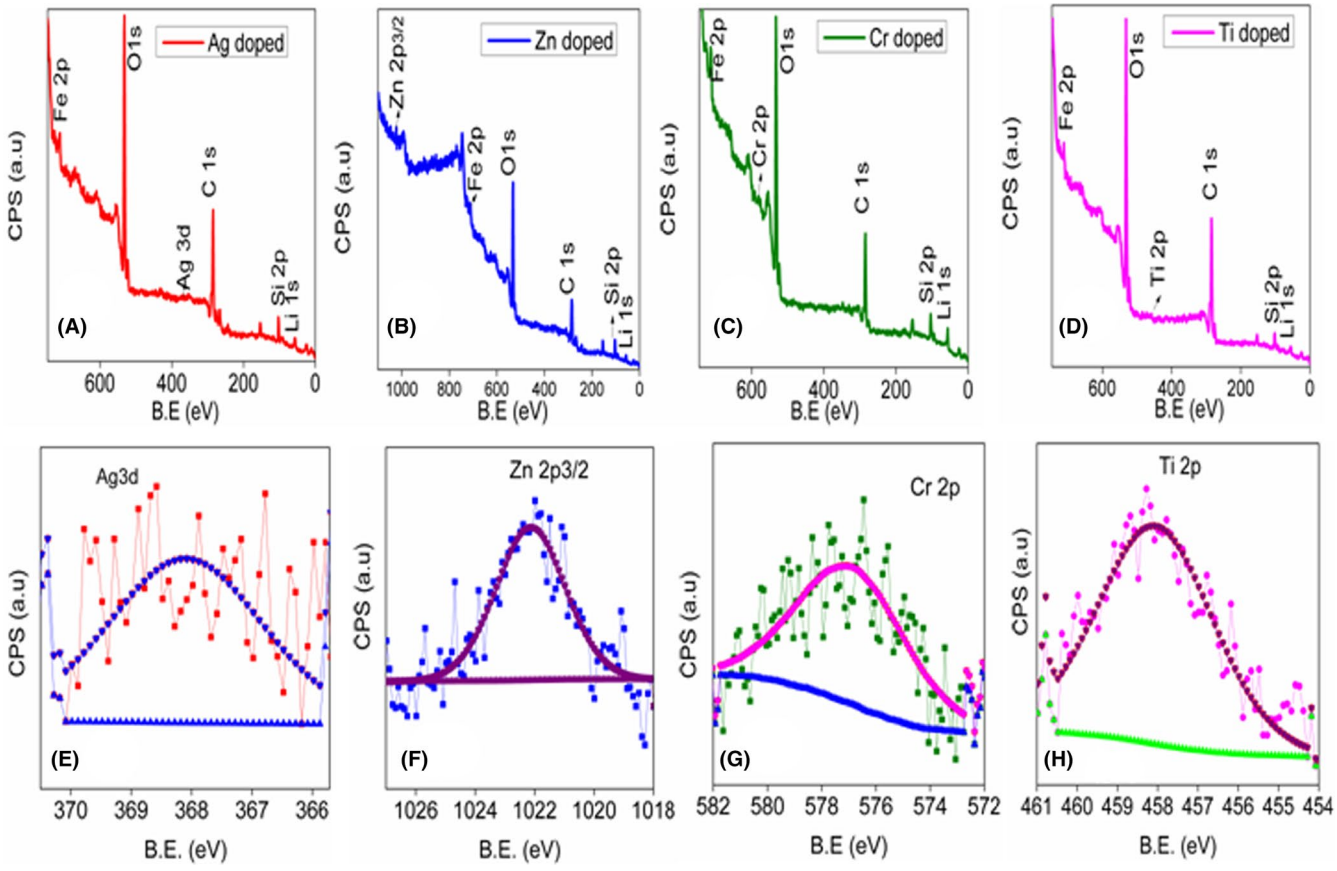

FIGURE 2 XPS survey spectra (A-D) of cations (Ag^{1+}, Zn^{2+}, Cr^{3+}, and Ti^{4+})-doped LFSO/C samples; XPS spectra for (E) Ag3*d*, (F) Zn2*p*, (G) Cr2*p*, and (H) Ti2*p* related peaks in Ag^{1+}, Zn^{2+}, Cr^{3+}, and Ti^{4+}-doped LFSO/C cathodes

LFSO/C has been estimated by the XPS peak area calculation using the CASA XPS Software and tabulated in Table 1. From Table 1, the estimated content of dopant elements Ag, Zn, Cr, and Ti at Fe site in the LFSO/C sample is 0.671, 1.170, 1.172, and 1.169 (at.%), respectively. The results reveal that the mole ratio of the (Zn^{2+}, Cr^{3+}, and Ti^{4+}) cations to Fe is determined as 1:7.47, 1:7.45, and 1:7.48; whereas the mole ratio for Ag-doped LFSO/C sample is determined as 1:13.13. In the Ag-doped LFS/O, the observed difference in molar ratio might be attributed to the higher ionic radii (1.26Å) of Ag in comparison with Fe element having low ionic radii (0.76Å).

The FTIR spectra of doped samples exhibit almost similar vibrational bands that occur in the LFSO/C, as shown in Figure S2. The vibrational bands noticed at 880 and 933 cm^{-1} in LFSO/C are attributed to the characteristic

TABLE 1 at.% of the dopant elements (Ag^{1+}, Zn^{2+}, Cr^{3+}, and Ti^{4+}) that present in the LFSO/C estimated from XPS spectra using CASA XPS Software

	Atomic percentage (%)								
Samples	**Li**	**Fe**	**Si**	**O**	**Ag**	**Zn**	**Cr**	**Ti**	**C**
Li_2FeSiO_4/C	20.30	9.60	9.30	49.50	—	—	—	—	11.30
$Li_2Fe_{0.9}Ag_{0.1}SiO_4/C$	21.63	8.88	10.62	46.23	0.67	—	—	—	11.94
$Li_2Fe_{0.9}Zn_{0.1}SiO_4/C$	20.42	8.74	8.97	50.31	—	1.17	—	—	10.37
$Li_2Fe_{0.9}Cr_{0.1}SiO_4/C$	19.57	8.84	11.51	48.43	—	—	1.172	—	10.55
$Li_2Fe_{0.9}Ti_{0.1}SiO_4/C$	20.43	8.75	9.96	48.53	—	—	—	1.169	11.34

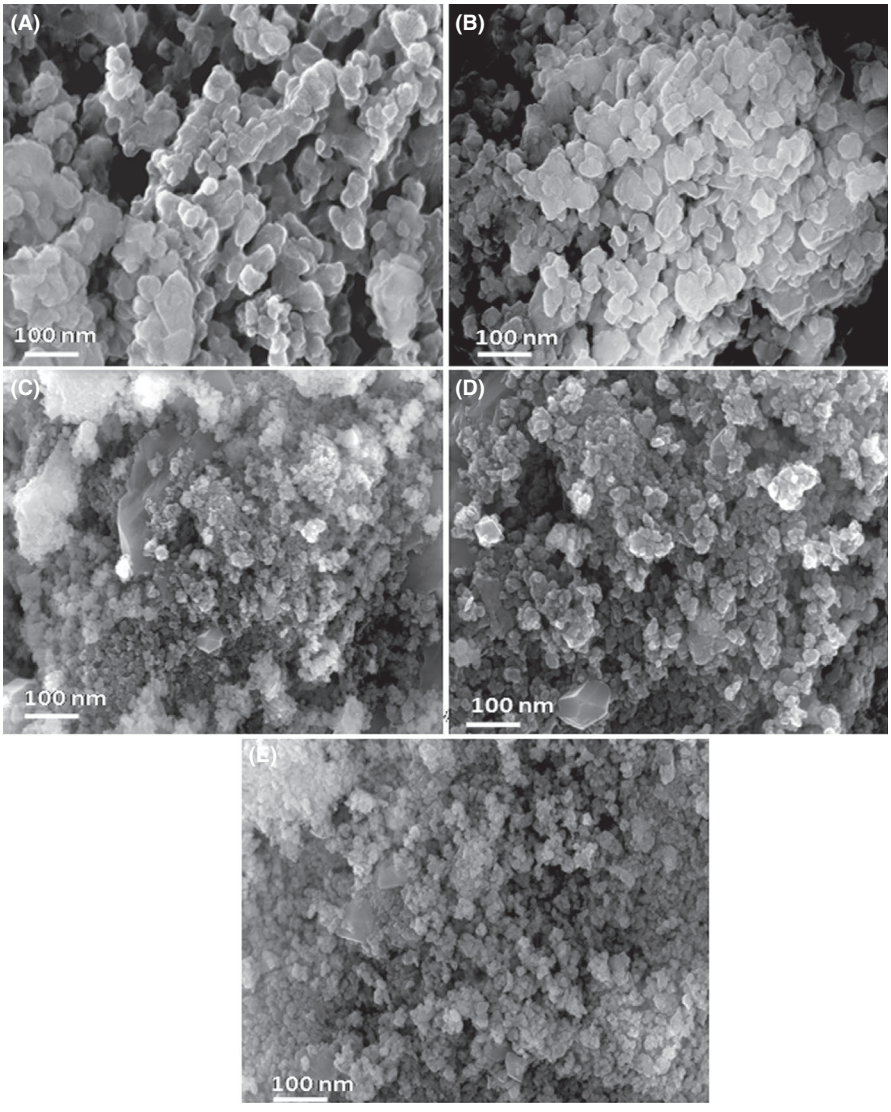

FIGURE 3 FE-SEM micrographs of bare and doped samples: (A) LFSO/C, (B) $Li_2Fe_{0.9}Ag_{0.1}SiO_4/C$, (C) $Li_2Fe_{0.9}Zn_{0.1}SiO_4/C$, (D) $Li_2Fe_{0.9}Cr_{0.1}SiO_4/C$, and (E) $Li_2Fe_{0.9}Ti_{0.1}SiO_4/C$ samples

stretching vibration of $(SiO_4)^{4-}$ group.[25] The minor peaks observed at 529 and 577 cm^{-1} are due to the possible bending vibration of the tetrahedron $(SiO_4)^{4-}$ and a peak at 457 indicates the stretching mode of Li–O tetrahedron in the LFSO/C.[16,26] The bare LFSO/C cathode exhibited the stretching modes (ν_3) at 880 and 933 cm^{-1} whereas the Ag^+, Zn^{2+}, Cr^{3+}, and Ti^{4+}-doped LFS/O samples (Figure S2) exhibit vibrational peaks at 880, 924, 882, and 938, and 900 cm^{-1} are also ascribed to the characteristics stretching vibration (ν_3) of $(SiO_4)^{-4}$ in the LFSO/C.[25] These bands are slightly shifted toward the low and high wavenumber which associated with changes in the local environment (LiO_4, FeO_4, and SiO_4 tetrahedrons orientation) due to the cations doping. The peak shift or broadening in the doped LFSO/C sample is attributed to the cations substitution and ordering in the silicate structures.[25–27] The vibrational modes present in the samples at 1440, 1493, and 1600 cm^{-1} are (Figure S2A-D) assigned to the small amount of Li_2CO_3 formed on the surface of the sample due to air exposure.[6] The Li_2CO_3 phase that occurs in the samples has not been reflected in the XRD pattern, due to its presence only in trace amounts.[28]

The FE-SEM micrograph of LFSO/C sample (Figure 3A) shows the uniform morphology with slightly aggregated spherical nanoparticles, whereas the Ag-doped LFSO/C material displays highly aggregated nanoparticles as shown in Figure 3B. The morphology of the LFSO/C is altered when Zn^{2+}, Cr^{3+}, and Ti^{4+}-doped into the host cage as evidenced from Figure 3C-E. The Zn^{2+}, Cr^{3+}-doped LFSO/C also show agglomerated particles. The $Li_2Fe_{0.9}Ti_{0.1}SiO_4$/C nano cathode possessed an aggregation of individual spherical particles with low particle size dispersed over the surface. The FE-SEM result implicates that, there is no obvious difference in morphology after substitution of cations, but Ti-doped LFSO/C shows less agglomeration and smaller particle size. The presence of the Ag, Zn, Cr, and Ti in the LFSO/C nanostructure has been ensured by EDAX spectra as depicted in Figure S3A-E. The uniform distribution of Ti on the surface of LFSO/C has been elucidated by EDS mapping as shown in Figure S3F,G.

The accurate particle size of the samples has been calculated using imageJ software from TEM images of bare, Ag^{1+}, Zn^{2+}, Cr^{3+}, and Ti^{4+}-doped LFSO/C nanocathode, as shown in Figure 4A1-A5. The particle size was determined for all the samples considering the full area of TEM images and reported the average particle size as 29, 38, 21, 24, and 26 nm for bare and Ag^+, Zn^{2+}, Cr^{3+}, and Ti^{4+}-doped LFSO/C samples, respectively. The grain size and morphology of the LFSO/C samples have been modified by substitution of different cations which is in agreement with the SEM and XRD analysis. The structure of the LFSO/C is further confirmed by HRTEM with SAED data. Figure

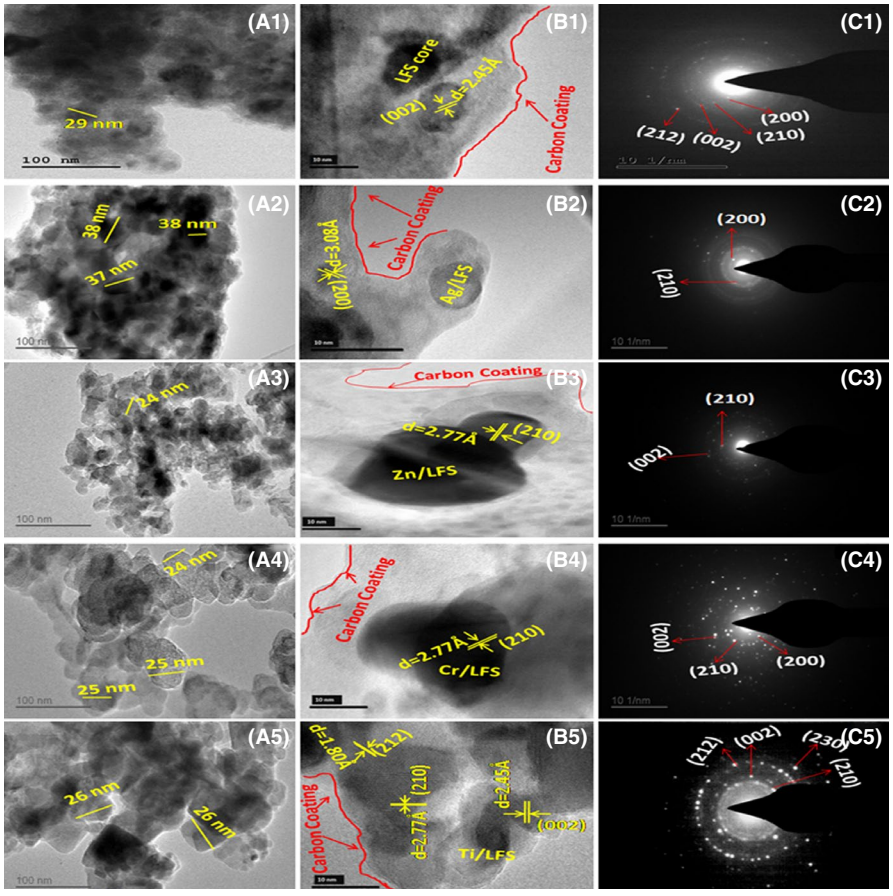

FIGURE 4 TEM, HR-TEM micrographs, and SAED pattern of bare and doped samples: (A1, B1, C1) Li_2FeSiO_4/C, (A2, B2, C2) $Li_2Fe_{0.9}Ag_{0.1}SiO_4$/C, (A3, B3, C3) $Li_2Fe_{0.9}Zn_{0.1}SiO_4$/C, (A4, B4, C4) $Li_2Fe_{0.9}Cr_{0.1}SiO_4$/C, and (A5, B5, C5) $Li_2Fe_{0.9}Ti_{0.1}SiO_4$/C

4B1-B5 shows the lattice images and the corresponding SAED pattern of the orthorhombic ($Pmn2_1$) LFSO/C as depicted in Figure 4C1-C5. As seen from SAED pattern, the d-spacings are obtained as 0.308, 0.277, 0.245, and 0.180 nm for the bare LFSO/C, which can be clearly indexed to the (200), (210), (002), and (212) crystallographic planes of orthorhombic LFSO/C. The d-spacing obtained from SAED is well matched with *d*-spacing of *hkl* planes from XRD pattern (0.3078, 0.2698, 0.2389, and 0.1834 nm). This structural inference obtained by SAED is consistent with that obtained from Rietveld refined XRD pattern which ensured that the cations-doped LFO/C possessed the same orthorhombic structure. The cations (Ag^{+}, Zn^{2+}, Cr^{3+}, and Ti^{4+})-doped LFSO/C also display similar (*hkl*) planes of the orthorhombic LFSO/C. Among these, Ti-doped LFSO/C shows the well-resolved diffraction rings with higher intensity diffracted spots when compared to other samples, corresponding to almost all (hkl) planes ((200), (210), (002), and (212)) of the orthorhombic phase in Ti-incorporated LFSO/C nanodomains which ensure good crystallinity of the sample. In addition, the TEM micrographs clearly show the uniform carbon encapsulation of the sample around the individual nanoparticles. The nanocrystalline domains with lattice fringes and the carbon encapsulated non-crystalline domains are clearly differentiated in the SAED pattern. The thin uniform carbon encapsulation around the well-differentiated individual particles as obtained in Ti-doped LFSO/C is reported to be a highly desirable feature for a cathode material for its enhanced electronic conductivity [29].

3.2 | Conductivity study

The impact of the cations (Ag^{1+}, Zn^{2+}, Cr^{3+}, and Ti^{4+}) doping on the electrical properties of LFSO/C nano cathode has been explored by AC impedance analysis. The conductivity of the material mainly depends on the type of dopants and their ionic radius, grain, grain boundary effects, and temperature. Figure 5A shows the Nyquist plot of LFSO/C and $Li_2Fe_{0.9}M_{0.1}SiO_4/C$ (M = Ag^{1+}, Zn^{2+}, Cr^{3+}, and Ti^{4+}) cathode material at room temperature. The Nyquist plots have been fitted to an equivalent circuit consisting of two (R_gCPE_g)($R_{gb}CPE_{gb}$) elements with one W1(Z_w) element in series, which attributed to the (g) grain, (gb) grain boundary, and material/electrode contribution, where R denoted a resistance and CPE is the constant phase element in parallel. The (W1) (inset picture in Figure 5A) has been used to make a better fit of the low-frequency electrode spike which is due to the Warburg diffusion of Li ions in the cathode material and the charge built up at the electrodes.[30–32] The plots show a combined high- and low-frequency semicircle for all the samples suggesting that the conductivity of the sample derives mainly from the grain and grain-boundary contributions.

The relaxation frequency (f_{max}), relaxation time (τ), and the jumping probability (P) of the samples have been calculated using the equations S1, S2, S3, and S4 and tabulated in Table S2. The $Li_2Fe_{0.9}Ti_{0.1}SiO_4/C$ sample possesses

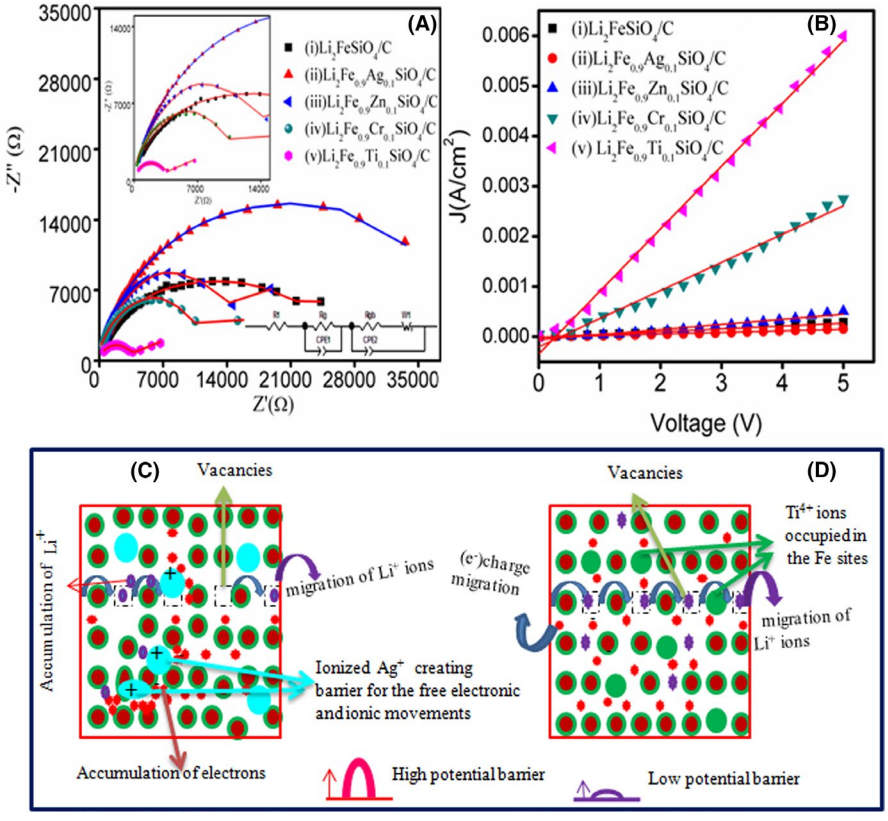

FIGURE 5 (A) Nyquist plots: (i) Ag|LFSO/C|Ag, (ii) Ag|$Li_2Fe_{0.9}Ag_{0.1}SiO_4$/C|Ag, (iii) Ag|$Li_2Fe_{0.9}Zn_{0.1}SiO_4$/C|Ag, (iv) Ag|$Li_2Fe_{0.9}Cr_{0.1}SiO_4$/C|Ag, and (v) Ag|$Li_2Fe_{0.9}Ti_{0.1}SiO_4$/C|Ag electrodes; (B) *J-V* curves with area of 0.2826 cm^2 and average thickness of 0.1192 cm; Schematic representation showing the ionic and electronic migration in (C) Ag^{+}-doped and (d) Ti^{4+}-doped LFSO/C

the highest jumping probability (5.83×10^7 per unit time), leading to a high electrical conductivity in the sample. The calculated grain and grain-boundary conductivity of samples are presented in Table S3. The room temperature total conductivity of LFSO/C sample is 4.66×10^{-5} S cm^{-1} which is far better than the reported value (2.8×10^{-8} S cm^{-1}) in the literature.[33,34] Among all the samples, the $Li_2Fe_{0.9}Ti_{0.1}SiO_4$/C sample exhibits an excellent total conductivity of 1.20×10^{-4} S cm^{-1} which is one order of magnitude higher than that of LFSO/C sample. The $Li_2Fe_{0.9}Ag_{0.1}SiO_4$/C sample possessed lower conductivity compared to all other samples, which may be due to the higher ionic radius (1.12 Å) of the Silver for its proper incorporation into the host matrix. The Ag containing sample when using Ag paste as contact electrode did not show any spike region due to the absence of blocking effect. Since the Ag paste has been utilized as the contact electrode, in Ag-doped sample different blocking electrodes has been attempted to obtain most reasonable values in conductivity. The respective curves with its Z-view fitted data have been included as supplementary information in Figure S5. The change in conductivity has been tabulated in Table S3. There is no major change in the grain and grain-boundary conductivity when it is compared with the sample used with Ag paste as contact electrode.

Further, the electronic conductivity of the pure and cations doped LFSO/C samples have been directly determined from I-V characteristic curves (Figure 5B) with a potential range 0.01V to 5V using dynamic potential scanning (DPS) method as recently reported in literature.[34] The area and average thickness of the samples have been determined as 0.2826 cm2 and 0.1192 cm, respectively. The electronic conductivity of the samples has been calculated using the equation S7 and tabulated in Table S3. The $Li_2Fe_{0.9}Ti_{0.1}SiO_4$/C exhibits good electronic conductivity of 6.56×10^{-5} S cm^{-1} which is higher than the previous report,[34] it is attributed to the uniform carbon coating on the sample. The variation in the conductivity of the LFSO/C and $Li_2Fe_{0.9}M_{0.1}SiO_4$/C (M = Ag^{1+}, Zn^{2+}, Cr^{3+}, and Ti^{4+}) cathodes is amenable with the change in the grain size of the particles. The decrease in the ionic conductivity of the $Li_2Fe_{0.9}Ag_{0.1}SiO_4$/C is due to the higher agglomeration of nanoparticles when compared with the bare and doped LFSO/C samples. The low crystallite size and the high degree of crystallinity facilitate an increase in hopping rate and jumping probability, which led to the highest total conductivity in $Li_2Fe_{0.9}Ti_{0.1}SiO_4$/C sample.

The variations in resistivity with dopants and grain size can be explored by carrier trapping model,[35] which suggests the trapped charges near the grain boundary causes a depletion region near the grain boundary. The monovalent (Ag^{1+}) ion substitution at the Fe^{2+} ion site decreases the electrical mobility due to the reduction in available free electrons and increasing ionized impurity scattering. Hence, the number of electrons around the oxygen is reduced, and the highly electronegative oxygen captures the free charge carriers in the localized trapped states. The trapped state near the grain boundary acts as potential barriers for the Li-ion movement. This potential barrier hinders the charge carrier transport between the grains, which reduces the mobility of the charge carrier.[36] Schematic representation showing the ionic and electronic migration in (C) Ag^+-doped and (D) Ti^{4+}-doped LFSO/C has been provided in Figure 5C,D. The tetravalent substitution of Fe atom by Ti atoms increases the electronic concentration, which enhances the electronic conductivity of the $Li_2Fe_{0.9}Ti_{0.1}SiO_4$/C sample. This emphasizes that the Titanium (Ti^{4+}) doping is an effective strategy to enhance the electrical performance of the LFSO/C nano cathode materials.

3.3 | Electrochemical performances

The electrochemical performance of LFSO/C and $Li_2Fe_{0.9}M_{0.1}SiO_4$/C (M = Ag^{1+}, Zn^{2+}, Cr^{3+}, and Ti^{4+}) cathodes has been recorded using Cyclic Voltammetry (CV) (Figure 6A-E) in an aqueous electrochemical system with 1M Li_2SO_4 electrolyte. The CV profiles were recorded at different scan rates from 1 to 5 mV s^{-1} over the potential range of −0.6 to 0.8 V versus SCE. The CV curve of LFSO/C at different scan rates is depicted in Figure 6A, which shows a single pair of redox peaks. It is observed that the electrode material exhibits Lithium intercalation/de-intercalation kinetics. The anodic peak at 361 mV vs SCE at 1 mV s^{-1} is corresponding to the oxidation of Fe ions during the extraction of lithium ions from LFSO/C. The cathodic peak at 102 mV vs SCE at 1 mVs^{-1} is assigned to the reduction in Fe ions accompanied by the insertion of Li-ion into LFSO/C material. The redox peak potential difference in bare LFSO/C is 259 mV. The potential difference between anodic and cathodic peaks is the major factor for exploring the electrochemical reversibility of an electrode material.[37] For all the scan rates, nearly symmetrical redox peaks can be observed. However, the oxidation-reduction peaks increase with an increase in the scan rates from 1 to 5 mV s^{-1}.

Figure 6B presents typical CV curves of $Li_2Fe_{0.9}Ag_{0.1}SiO_4$/C, it is noted that the obtained CV curves are not similar to the LFSO/C material, the oxidation and reduction peaks are shifted to a higher potential with an increase in scan rate to 5 mV s^{-1}. The CV curves for the $Li_2Fe_{0.9}Ag_{0.1}SiO_4$/C at a scan rate of 1 mV s^{-1} show a peak potential difference of 361 mV, which is far higher than that of LFSO/C. The result reveals that the Ag doping negatively influenced the redox reversibility due to low electrical conductivity and structural re-arrangement, which causes the quasi-reversible behavior of the sample. It is noted that the Zn- and Cr-incorporated LFSO/C samples show low oxidation and reduction peak current when compared with the LFSO/C material as shown in Figure 6C,D. The $Li_2Fe_{0.9}Ti_{0.1}SiO_4$/C sample also follows the symmetrical redox CV curves with well-resolved anodic and

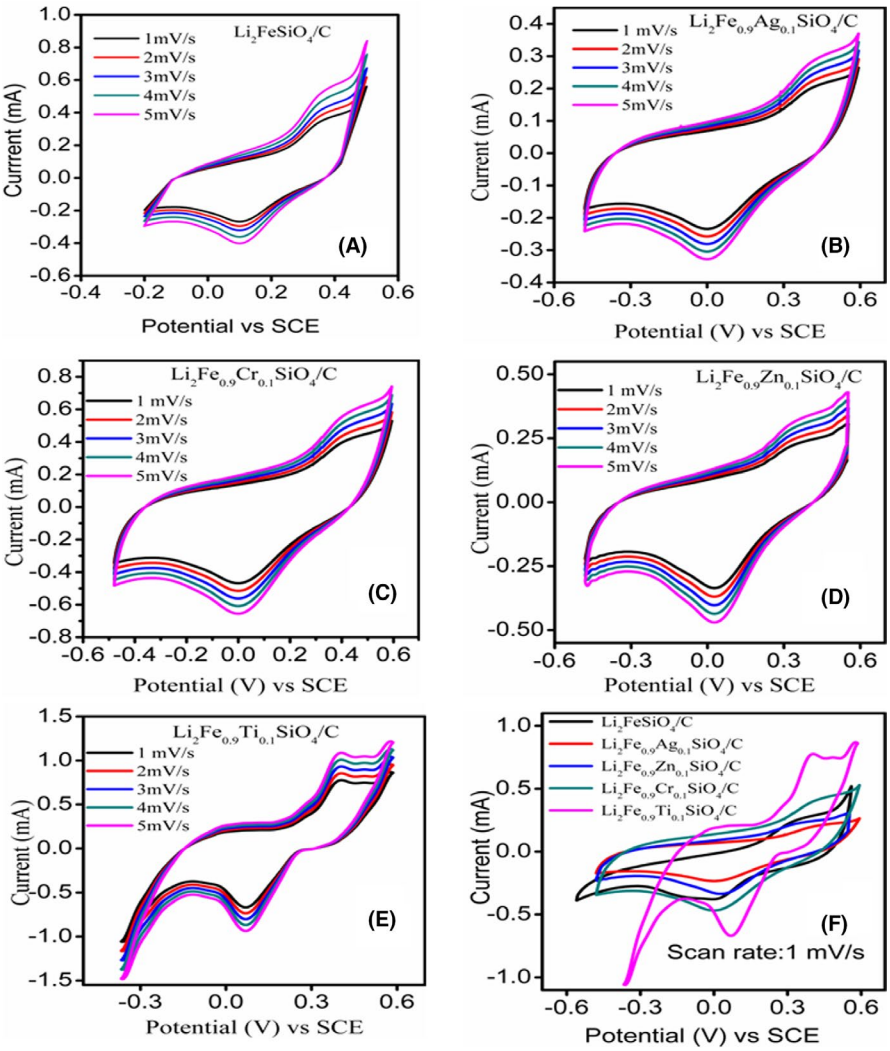

FIGURE 6 CV curves (A) LFSO/C, (B) $Li_2Fe_{0.9}Ag_{0.1}SiO_4/C$, (C) $Li_2Fe_{0.9}Zn_{0.1}SiO_4/C$, (D) $Li_2Fe_{0.9}Cr_{0.1}SiO_4/C$, and (E) $Li_2Fe_{0.9}Ti_{0.1}SiO_4/C$ electrodes with different scan rates from 1 to 5 mV s^{-1}, (F) combined CV curves for all the samples at 1 mV s^{-1}

cathodic peaks and its peak current is more prominent than all other samples as depicted in Figure 6E. The CV curves of $Li_2Fe_{0.9}Ti_{0.1}SiO_4/C$ at a scan rate of 1 mV s^{-1} gives the low potential difference of 196 mV, which reveal that the Ti-doped LFSO/C exhibits better redox kinetics than all other samples. The low potential separation is an indication of better electrochemical reversibility.[38] The single pair of redox peaks corresponding to the Fe^{2+}/Fe^{3+} redox that couple has been observed in the doped LFSO/C.[38] Since there is no other oxidation or reduction hike observed in the CV curve, it is clear that the dopant ions are not participating directly in the redox activity of LFSO/C.[14,39] However, Ag containing sample exhibits higher potential difference at a low scan rate and lower peak current than that of the other samples, which demonstrates its poor electrochemical performance.

The Zn- and Cr-doped samples exhibit slightly higher potential difference than that of $Li_2Fe_{0.9}Ti_{0.1}SiO_4/C$ material, however, which is lower than that of parent and Ag-containing LFSO/C sample. A combined plot at 1mVs^{-1} has been provided to analyze the peak area of the CV plot (Figure 6F), which clearly shows the impact of cations doping on the electrochemical activity of LFSO/C electrode. In addition to that, the CV curve of $Li_2Fe_{0.9}Ti_{0.1}SiO_4/C$ displays the large redox peak area with high peak current (Figure 6F), which effectively enrich the specific capacity of cathode active material. The CV measurement at different scan rates has been used to estimate the Li-ion diffusion coefficient of LFSO/C and $Li_2Fe_{0.9}M_{0.1}SiO_4/C$ ($M = Ag^{1+}$, Zn^{2+}, Cr^{3+}, and Ti^{4+}) samples. The Randles-Sevcik equation (S8) can be used to explore the impact of scan rate on redox peak current (i_p).[38,40] The linear plot of peak current (i_p) and square root of scan rate ($V^{1/2}$) (see Figure S6) is an indication of a high electrochemical reversible redox process. The results revealed that the samples are exhibiting quasi-reversible nature. The peak current is proportional to different scan rates, which means that the Li-ion de-intercalation/intercalation processes occurred in the electrode are diffusion-controlled.[9] The $Li_2Fe_{0.9}Ti_{0.1}SiO_4/C$ sample exhibits an anodic and cathodic diffusion coefficient of 6.34×10^{-12} and 5.03×10^{-12} cm^2 s^{-1} which is far better than the bare and Ag^{1+}, Zn^{2+}, Cr^{3+}-doped LFSO/C nano cathodes (Table 2). The obtained diffusion coefficient for $Li_2Fe_{0.9}Ti_{0.1}SiO_4/C$ is

also higher than the reported value.[22] The Ti^{4+} ion is not involved in the oxidation or reduction during the intercalation/de-intercalation processes, which is in agreement with the previous report.[40] However, it proliferates the redox process and the interaction of the $Fe^{2+/}Fe^{3+}$ redox couple, which evidences for the synergic interaction between the dopant and the host matrix. This, in turn, facilitates to preserve more diffusion path for Lithium-ion intercalation, which enhances the electrochemical activity.

The EIS plot of the pure and metal ions-doped LFSO/C cathode is depicted in Figure 7A which clearly shows a high-frequency semicircle with a low-frequency spike. The observed semicircle at higher frequency range is attributed to charge transfer resistance (R_c). The charge transfer resistance of the samples has been differentiated by fitting the original data using the most suited equivalent circuit model. The charge transference is associated with resistance against the movement of Li^+ ions from the active electrode to the reference electrode through the electrolyte. The R_e represents the combination of ionic resistance of electrolyte and intrinsic resistance of the cathode active material which determines the charge-discharge rate performance of the electrode. The estimated EIS parameters were listed in Table 2. The Ti-doped LFSO/C sample exhibits low charge transfer resistance R_c (184 Ω) when compared to bare and Ag, Zn, Cr-doped LFSO/C samples, which substantiate that the sample can deliver better electrochemical performance when compared with other samples. The diffusion coefficient (D_{Li+}) and the

TABLE 2 Fitted parameters for EIS and diffusion coefficient for pure and cations (Ag^{1+}, Zn^{2+}, Cr^{3+}, and Ti^{4+}) ions-doped LFSO/C

					D_{Li+} ($cm^2\ s^{-1}$)		
						Obtained from CV curves	
Samples	R_e (Ω)	R_c (Ω)	σ_w ($cm^2\ s^{-1/2}$)	i ($mA\ cm^{-2}$)	Obtained from EIS	Anodic	Cathodic
LFSO/C	2.12	330	29.12	7.91×10^{-5}	1.14×10^{-13}	7.38×10^{-13}	8.22×10^{-13}
Ag-FSO/C	2.36	397	38.15	6.58×10^{-5}	0.62×10^{-13}	4.49×10^{-13}	4.61×10^{-13}
Zn-LFSO/C	1.19	286	26.34	9.13×10^{-5}	1.39×10^{-13}	7.52×10^{-13}	9.86×10^{-13}
Cr-LFSO/C	1.73	243	18.45	1.07×10^{-4}	2.83×10^{-13}	9.98×10^{-13}	1.91×10^{-12}
Ti-LFSO/C	1.11	184	9.12	1.42×10^{-4}	1.16×10^{-12}	6.34×10^{-12}	5.03×10^{-12}

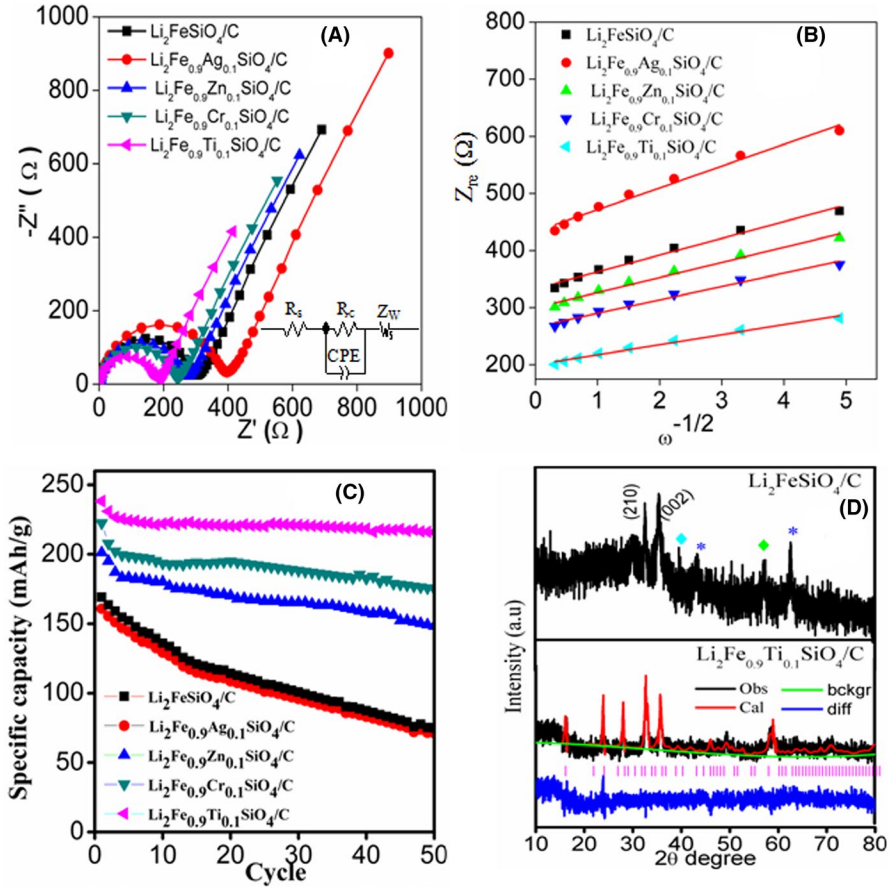

FIGURE 7 (A) EIS plots and (B) relationship between Z' and $\omega^{-1/2}$ in low frequency region of bare and Ag^{1+}, Zn^{2+}, Cr^{3+}, and Ti^{4+}-doped Li_2FeSiO_4/C nano electrodes. (C) The discharge capacity of pure and cations (Ag^{1+}, Zn^{2+}, Cr^{3+}, and Ti^{4+})-doped Li_2FeSiO_4/C nano cathodes. (D) Post XRD pattern of LFSO/C and $Li_2Fe_{0.9}Ti_{0.1}SiO_4$/C

exchange current density (i_d) have been calculated using Figure 7B and presented in Table 2 (details of the calculations has been included in the supplementary information, see Section S8). The diffusion coefficient and the exchange current density of the $Li_2Fe_{0.9}Ti_{0.1}SiO_4$/C are 1.16×10^{-12} cm^2 s^{-1} and 1.42×10^{-4} mA cm^{-2}, the (D_{Li+}) is comparable with that obtained from CV curves. The particle size forms one of the plausible reason behind the improvement of electrochemical performance since smaller nanoparticles have large surface to volume ratio, and can effectively reduce the grain-boundary resistance and charge transfer resistance to improve the diffusion coefficient of Li-ions and high exchange current density in Ti-doped LFSO/C cathode,[41] which positively influences the specific capacity of the sample.

The cycling stability of bare and cations-doped LFSO/C cathodes have been explored by galvanostatic charge-discharge test over 50 cycles. All the samples were cycled with same current rate of 1 C (In a typical sample, applied current 1.0292 mAh g^{-1} for an active mass of the electrode: 0.0031 g) where the theoretical capacity has been assumed as 332 mAh g^{-1} for two lithium-ion transfer per formula unit. The specific capacity of the LFSO/C and $Li_2Fe_{0.9}M_{0.1}SiO_4$/C (M = Ag^{1+}, Zn^{2+}, Cr^{3+}, and Ti^{4+}) cathodes has been estimated over 50 cycles as shown in Figure 7C. The LFSO/C possessed an initial specific capacity of 162 mAh g^{-1} and 89 mAh g^{-1} after 50 cycles. It shows severe capacity fading after the first cycle during charging and discharging processes. The Ag-doped sample exhibits a lower specific capacity than that of bare material. The Zn- and Cr-doped sample possessed slightly higher capacity than the LFSO/C, but exhibits capacity fading after 20 cycles. It is noted that the $Li_2Fe_{0.9}Ti_{0.1}SiO_4$/C material provides an excellent initial specific capacity of 242 mAh g^{-1} and 226 mAh g^{-1} after 50 cycles with a capacity retention of 93.38%. The capacity fading of LFSO/C nano cathode can be ascribed to the phase change or even structure fracture during the intercalation and de-intercalation of Li-ions.[42,43]

In order to understand the structural deformation after multiple electrochemical charge discharge cycles, the XRD pattern of the pure LFSO/C and Ti-incorporated LFSO/C have been recorded after the electrochemical test (Figure 7D). The LFSO/C exhibits only two peaks of orthorhombic structure and rest of the peaks are indexed to the emergence of major phases such as: $LiFeO_2$ (Jcpds:89-7118, indicated as:*) and (Fe_2O_3 (Jcpds:88-2359, indicated as: ♦) which reveal that the bare sample undergoes structural fracture or changes to be amorphous after multiple charge-discharge process. The $Li_2Fe_{0.9}Ti_{0.1}SiO_4$/C sample maintains more or less all the peaks that present before cycling in the post XRD pattern which are well indexed to the orthorhombic structure ($Pmn2_1$).

The lattice parameters obtained from the Rietveld refined post XRD pattern of $Li_2Fe_{0.9}Ti_{0.1}SiO_4$/C (Figure 7D), gives the values: a = 6.312, b = 5.389 and c = 4.987 Å, which are comparable with the same before cycling (a = 6.265, b = 5.361 and c = 4.915 Å). The comparatively less changes in the lattice parameter values in the post XRD pattern of $Li_2Fe_{0.9}Ti_{0.1}SiO_4$/C, ascertains that the Ti doping could effectively preserve the structural collapse or amorphization during the charge-discharge process. This major obstacle has been overcome by the proper doping of Ti^{4+} in the Fe site to enhance the coupling effect among the tetrahedral sites by a strong d-orbital hybridization, which can act as spring to hold LiO_4, FeO_4, and SiO_4 tetrahedrons and prohibit structural fracture[22] during charge-discharge processes. Furthermore, Ti^{4+} could maintain the crystallinity of the host sample during the electrochemical reaction, thus it can stabilize the crystal lattice and enhance the cycling stability of LFSO/C. When Ag^{1+} with higher ionic radii is incorporated to the Fe sites, due to its larger size it limits the possible facile intercalation pathways of the Li-ion. Along with this, the larger impurity dopant also causes the impurity scattering of the free ions, which in turn again decreases the number of free ions moving through the crystal (Figure 5C,D). The structural deformation that causes due to the heavier ionic particle incorporation also acts as a hindrance for maintaining the initial capacity of the LFSO/C sample, this, in turn, results in capacity fading of the sample. The present study suggests that the valence state of dopants can effectively affect the electrical and electrochemical performance of LFSO/C cathode. The electrochemical performance of LFSO/C increases with an increase in valency (Ag^{1+}, Zn^{2+}, Cr^{3+}, and Ti^{4+}) of the dopants. The n-type Ti^{4+} (higher valence state in comparison to other dopants) embedded LFSO/C provides an excellent electrical and electrochemical performance with better electrical contact between the electrode/electrolyte interface which increases the electrochemical cyclability.

4 | CONCLUSION

The influence of transition metal ions (Ag^{1+}, Zn^{2+}, Cr^{3+}, and Ti^{4+}) substitution on the structural, electrical, and electrochemical activities of the LFSO/C nanostructures has been systematically investigated. The XRD and HR-TEM (SAED) result revealed that LFSO/C and $Li_2Fe_{0.9}M_{0.1}SiO_4$/C (M = Ag^{1+}, Zn^{2+}, Cr^{3+}, and Ti^{4+}) cathodes possessed the orthorhombic structure (S.G-$Pmn2_1$). The XPS analysis demonstrated the presence of the dopants (Ag^{1+}, Zn^{2+}, Cr^{3+}, and Ti^{4+}) and their composition in the sample. The $Li_2Fe_{0.9}Ti_{0.1}SiO_4$/C sample exhibits better anodic and cathodic diffusion coefficients of 6.34×10^{-12} and 5.03×10^{-12} cm^2 s^{-1} than that of bare and Ag^{1+}, Zn^{2+}, Cr^{3+}-doped LFSO/C nanostructures. The Ti^{4+}-embedded LFSO/C nanomaterial delivers an excellent initial specific capacity of 242 mAh g^{-1} and maintains a capacity of 226 mAh g^{-1} after 50 cycles (with 6.62% fading with respect to the initial capacity). The tetravalent

substitution of Fe by Ti could introduce defects in the lattice and creates an additional conduction channel to facilitate the facile redox activity, which effectively alleviates structure collapse in Li_2FeSiO_4 nanostructure during the charge-discharge process.

ACKNOWLEDGMENT

Mr P. Sivaraj thanks the Council of Scientific Industrial Research (CSIR), Govt. of India, New Delhi, for providing the necessary financial support through the Senior Research Fellowship (SRF) (File no:09/0472(0181)2018-EMR-I) to carry out the work.

ORCID

Karuthedath Parameswaran Abhilash https://orcid.org/0000-0001-9469-3204

Paneerselvam Christopher Selvin https://orcid.org/0000-0002-3354-5790

REFERENCES

1. Islam MS, Dominko R, Masquelier C, Sirisopanaporn C, Armstrong AR, Bruce PG. Silicate cathodes for lithium batteries: alternatives to phosphates. J Mater Chem. 2011;27:9811–8.
2. Zhang L-L, Sun H-B, Yang X-L, Wen Y-W, Huang Y-H, Li M, et al. Study on electrochemical performance and mechanism of V-doped Li_2FeSiO_4 cathode material for li-ion batteries. Electrochim Acta. 2015;152:496–504.
3. Nyten A, Abouimrane A, Armand M, Gustafsson T, Thomas JO. Electrochemical performance of Li_2FeSiO_4 as a new Li-battery cathode material. Electrochem Commun. 2005;7:156–60.
4. Nyten A, Kamali S, Hanggstrom L, Gustafsson T, Thomas JO. The lithium extraction/insertion mechanism in Li_2FeSiO_4. J Mater Chem. 2006;16:2266–72.
5. Yang J, Zheng J, Kang X, Teng G, Hu L, Tan R, et al. Tuning structural stability and lithium-storage properties by d-orbital hybridization substitution in full tetrahedron Li_2FeSiO_4 nanocrystal. Nano Energy. 2016;20:117–25.
6. Thayumanasundaram S, Rangasamy VS, Seo JW, Locquet JP. A combined approach: polyol synthesis of nanocrystalline Li_2FeSiO_4, doping multi-walled carbon nanotubes, and ionic liquid electrolyte to enhance cathode performance in Li-ion batteries. Electrochim Acta. 2017;258:1044–52.
7. Qiu H, Yue H, Zhang T, Ju Y, Zhang Y, Guo Z, et al. Enhanced electrochemical performance of Li_2FeSiO_4/C positive electrodes for lithium-ion batteries via yttrium doping. Electrochim Acta. 2016;188:636–44.
8. Girish HN, Shao GQ. Advances in high-capacity Li_2MSiO_4 (M = Mn, Fe Co, Ni) cathode materials for lithium-ion batteries. RSC Adv. 2015;5(119):98666–86.
9. Zhang L-L, Duan S, Yang X-L, Liang G, Huang Y-H, Cao X-Z, et al. Insight into cobalt-doping in Li_2FeSiO_4 cathode material for lithium-ion battery. J Power Sources. 2015;274:194–202.
10. Wang YC, Zhao SX, Zhai PY, Li F, Nan CW. Solvothermal synthesis and electrochemical performance of Li_2MnSiO_4/C cathode materials for lithium ion batteries. J Alloys Compd. 2014;614:271–6.
11. Wagemaker M, Ellis BL, Lutzenkirchen HD, Mulder FM, Nazar LF. Proof of supervalent doping in olivine $LiFePO_4$. Chem Mater. 2008;20:6313–5.
12. Deng C, Zhang S, Yang SY, Fu BL, Ma L. Synthesis and characterization of $Li_2Fe_{0.97}M_{0.03}SiO_4$(M=$Zn^{2+}$, Cu^{2+}, Ni^{2+}) cathode materials for lithium ion batteries. J Power Sources. 2011;196:386–92.
13. Zhang S, Deng C, Fu BL, Yang SY, Ma L. Effects of Cr doping on the electrochemical properties of Li_2FeSiO_4 cathode material for lithium-ion batteries. Electrochim Acta. 2010;55:8482–9.
14. Qiu H, Yue H, Wang X, Zhang T, Zhang M, Fang Z, et al. Titanium-doped Li_2FeSiO_4/C composite as the cathode material for lithium-ion batteries with excellent rate capability and long cycle life. J Alloys Compd. 2017;725:860–8.
15. Sivaraj P, Nalini B, Abhilash KP, Lakshmi D, Christopher Selvin P, Balraju P. Study on the influences of calcination temperature on structure and its electrochemical performance of Li_2FeSiO_4/C nano cathode for lithium ion batteries. J Alloys Compd. 2018;740:1116–24.
16. Singh S, Mitra S. Improved electrochemical activity of nanostructured Li_2FeSiO_4/MWCNT composite cathode. Electrochim Acta. 2014;123:378–86.
17. Lu X, Wei H, Chiu H-C, Gauvin R, Hovington P, Guerfi A, et al. Rate-dependent phase transitions in Li_2FeSiO_4 cathode nanocrystals. Sci Rep. 2015;5:8599.
18. Dong Y, Zhang W-L, Wang C-M, Shi T, Chen LI. Synthesis of La-doped Li_2MnSiO_4 nano-particle with high-capacity via polyol-assisted hydrothermal method. Electrochim Acta. 2015;166:40–6.
19. Masese T, Tassel C, Orikasa Y, Koyama Y, Arai H, Hayashi N, et al. Crystal structural changes and charge compensation mechanism during two lithium extraction/insertion between Li_2FeSiO_4 and $FeSiO_4$. J Phys Chem C. 2015;119(19):10206–11.
20. Li L, Han E, Dou L, Zhu L, Mi C, Li M, et al. Enhanced electrochemical performance of Li_2FeSiO_4/C as cathode for lithium-ion batteries via metal doping at Fe-site. Solid State Ionics. 2018;325:30–42.
21. Biesinger MC, Lau LW, Gerson AR, Smart RS. Resolving surface chemical states in XPS analysis of first row transition metals, oxides and hydroxides: Sc, Ti, V, Cu and Zn. Appl Surf Sci. 2010;257:887–98.
22. Wu X, Zhao SX, Wei L, Deng H, Nan CW. Improving the structure stability and electrochemical performance of Li_2MnSiO_4/C cathode materials by Ti-doping and porous microstructure. J Alloys Compd. 2018;735:1158–66.
23. Zhang Z, Liu X, Wang L, Wu Y, Zhao H, Chen B, et al. Fabrication and characterization of carbon-coated Li_2FeSiO_4 nanoparticles reinforced by carbon nanotubes as high performance cathode materials for lithium-ion batteries. Electrochim Acta. 2015;168:8–15.
24. Jaen JA, Iglesias J, Munoz A, Tabares JA, Perez Alcazar GA. Characterization of magnesium doped lithium iron silicate. Croat ChemActa. 2015;88(4):487–93.
25. Zaghi K, Ait Salah A, Ravet N, Mauger A, Gendron F, Julien CM. Structural, magnetic and electrochemical properties of lithium iron orthosilicate. J Power Sources. 2006;160:1381–6.
26. Luo XY, Wang PP, Cheng X, Zhang Y, Huang LY. An orthogonal investigation of sulfur modified Li_2FeSiO_4 for lithium ion batteries. ECS Trans. 2018;85(13):235–46.

27. Yi J, Hou MY, Bao HL, Wang CX, Wang JQ, Xia YY. In-situ generation of Li_2FeSiO_4/C nanocomposite as cathode material for lithium ion battery. Electrochim Acta. 2014;133:564–9.
28. Yang J, Kang X, He D, Zheng A, Pan M, Mu S. Graphene activated 3D-hierarchical flower-like Li_2FeSiO_4 for high performance lithium-ion batteries. J Mater Chem A. 2015;168:16567–73.
29. Sun D, Wang H, Ding P, Zhou N, Huang X, Tan S, et al. In-situ synthesis of carbon coated Li_2MnSiO_4 nanoparticles with high rate performance. J Power Sources. 2013;242:865–71.
30. Irvine J, Sinclair DC, West AR. Electroceramics: characterization by impedance spectroscopy. Adv Mater. 1990;2(3):132–8.
31. Marrero-Lopez D, Canales-Vazquez J, Ruiz-Morales JC, Irvine J, Nunez P. Electrical conductivity and redox stability of $La_2Mo_{2-x}W_xO_9$ materials. Electrochim Acta. 2005;50(22):4385–95.
32. Orera A, Garcia-Alvarado F, Irvine J. Effect of Ti-substitution on the electrical properties of $MnNb_2O_6$-δ. Chem Mater. 2007;19:2310–5.
33. Kokalj A, Dominko R, Mali G, Meden A, Gaberscek M, Jamnik J. Beyond one-electron reaction in Li cathode materials: designing $Li_2Mn_xFe_{1-x}SiO_4$. Chem Mater. 2007;19:3633–40.
34. Liu L, Wang P, Li J, Shi G, Ma L, Zhao J, et al. Hydrothermal preparation and intrinsic transport properties of nanoscale Li_2FeSiO_4. Solid State Ion. 2018;320:353–9.
35. Saravanan R, Pukazhselvan D, Mahadevan CK. Studies on the synthesis of cubic ZnS quantum dots, capping and optical electrical characteristics. J Alloys Compd. 2012;517:139–48.
36. Ziang Y, Li Y, Yan M, Bahlawane N. Abnormal behaviors in electrical transport properties of cobalt-doped tin oxide thin films. J Mater Chem. 2012;22:16060–5.
37. Liu Y, Mi C, Yuan C, Zhang X. Improvement of electrochemical and thermal stability of $LiFePO_4$ cathode modified by CeO. J Electroanal Chem. 2009;628:73–80.
38. Georgijevi R, Vujkovi M, Guti S, Aliefendi M, Jugovi D, Mitri M, et al. The influence of synthesis conditions on the redox behaviour of $LiFePO_4$ in aqueous solution. J Alloys Compd. 2019;776:475–85.
39. Wu X, Zhao SH, Wei L, Zhao EL, Li JW, Nan CW. Improved structural reversibility and cycling stability of Li_2MnSiO_4 cathode material by the pillar effect of [TiO_x] polyanions. Chemistry Select. 2018;3:4047–57.
40. Yu YW, Fietzek C, Weydanz W, Donoue K, Inoue T, Kurokawa H, et al. Study of $LiFePO_4$ by cyclic voltammetry. J Electrochem Soc. 2007;154:253–7.
41. Shenouda AY, Sanad M. Synthesis, characterization and electrochemical performance of $Li_2Ni_xFe_{1-x}SiO_4$ cathode materials for lithium ion batteries. Bull Mater Sci. 2017;40:1055–60.
42. Kamon-in O, Klysubun W, Limphirat W, Srilomsak S, Meethong N. An insight into crystal, electronic, and local structures of lithium iron silicate (Li_2FeSiO_4) materials upon lithium extraction. Phys B. 2013;416:69–75.
43. Masese T, Orikasa Y, Tassel C, Kim J, Minato T, Arai H, et al. Relationship between phase transition involving cationic exchange and charge-discharge rate in Li_2FeSiO_4. Chem Mater. 2014;26(3):1380–4.

SUPPORTING INFORMATION

Additional supporting information may be found online in the Supporting Information section at the end of the article.

How to cite this article: Sivaraj P, Abhilash KP, Nalini B, Selvin PC, Goel S, Yadav SK. Insight into cations substitution on structural and electrochemical properties of nanostructured Li_2FeSiO_4/C cathodes. *J Am Ceram Soc*. 2019;00:1–13. https://doi.org/10.1111/jace.16805